# Collective molecular rotation in $D_2O$

David P. Shelton
*Department of Physics, University of Nevada, Las Vegas, Las Vegas, Nevada 89154-4002*

(Received 10 June 2002; accepted 26 August 2002)

The hyper-Rayleigh scattering (HRS) spectrum of liquid $D_2O$ was measured at 90° scattering angle with linearly polarized light (VV, HV, VH, and HH polarization geometries). The VV and HV spectral profiles are similar, but the HV and VH spectral profiles are very different. This can be accounted for by scattering from nonlocal modes of molecular reorientation. The local mode and the transverse nonlocal mode both result in Lorentzian spectral components with width increasing from 1.1 $cm^{-1}$ at $T=23$ °C to 3.3 $cm^{-1}$ at 80 °C. The spectrum due to the longitudinal nonlocal mode has width $<0.3$ $cm^{-1}$. A relatively weak and very broad collision-induced spectral component is also observed. The relative integrated intensities of the local, transverse and longitudinal components of the VH HRS spectrum are 21%, 45%, and 34%, indicating that molecular reorientation in water is predominantly a collective effect. © *2002 American Institute of Physics.*
[DOI: 10.1063/1.1514976]

## I. INTRODUCTION

Light scattering has been used as a tool to investigate the motion of molecules in liquids for almost a century.[1–3] The orientational and translational motions of the molecules result in spectral features at small frequency shifts, typically $<100$ $cm^{-1}$. The most prominent feature of the polarized scattered light spectrum is the Rayleigh–Brillouin triplet due to diffusive and propagating (longitudinal acoustic) density fluctuations of the fluid. The depolarized scattered light spectrum for a fluid of anisotropic molecules typically has a central Lorentzian peak ascribed to rotational diffusion of the molecules, riding on broad exponential wings due to fluctuations induced by intermolecular interactions during collisions. A characteristic central dip (Rytov dip) can occur due to coupling between molecular orientation and shear flow in the liquid.

Nonlinear light scattering experiments are interesting since they can reveal modes of motion that are invisible to linear light scattering. In particular, transverse and longitudinal polar modes of collective molecular motion produce hyper-Rayleigh scattering (HRS) spectra with distinctive polarization dependence.[4–7] HRS is allowed for both optic and acoustic modes provided the modes are polar. Since the acoustic phonons responsible for the Brillouin doublet are scalar density waves they do not contribute to the HRS spectrum. HRS with the polarization dependence characteristic of a transverse polar collective mode has recently been reported for acetonitrile.[5] The aim of the present experiments is to better understand such collective modes of molecular reorientation in liquids.

Water is a particularly interesting and important liquid, with a very extensive literature on its structure and properties.[8,9] Accurate *ab initio* calculations of the nonlinear optical properties of this molecule are also available to aid the analysis and interpretation of HRS measurements. This makes water a natural choice for further study of collective reorientation modes.

## II. HRS EXPERIMENT

The experimental apparatus and methods used in this work have been previously described.[10,11] The beam from a pulsed Nd:YAG laser operating at $\lambda=1064$ nm was focused into the liquid sample contained in a 1 cm fused silica fluorimeter cuvette placed in a thermostatic enclosure, and the scattered light near $\theta=90°$ and $\lambda=532$ nm was collected with an f/1.8 lens and analyzed by a grating spectrometer with calibrated spectral response. The incident beam in the sample had a waist diameter of 15 $\mu$m, and the pulses typically had a 1 kHz repetition rate, 100 ns duration, and 1 mJ energy. A visible-blocking glass filter (Schott RG-850) placed just before the laser focusing lens prevented second-harmonic light generated along the beam path from entering the sample region. The sample was reagent grade $D_2O$ (99.9 at % D) filtered through a 0.2 $\mu$m micropore filter. The polarization of the incident laser beam was controlled using a prism polarizer and an electronically controlled liquid crystal variable wave plate (LCVWP), while the polarization of the collected light was analyzed using a sheet polarizer mounted so that the polarization axis could be rotated rapidly by 90°.

The polarization geometry was either VV, HV, VH, or HH, where V (H) denotes the polarization direction perpendicular (parallel) to the horizontal scattering plane, and the first (second) letter refers to the incident (detected scattered) polarization. An electrical command pulse switches the apparatus rapidly (0.1 s) from one polarization geometry to another. Since accurate polarization ratios are critical to the analysis and interpretation of this work, spectra were acquired in matched pairs, for example, VV and HV, or HV and VH. The selected spectral region was scanned multiple times, alternating the polarization geometry on each successive scan, for 100–1000 scans (typically 4 min per scan). In this way, spectra with different polarization geometry were obtained under otherwise identical conditions.

The plan is to distinguish the HRS spectral components due to local or collective modes by their different polariza-

 

TABLE I. Polarization dependence of HRS intensities at 90° scattering angle for local and collective modes.

| Mode | $I_{VV}$ | $I_{HV}$ | $I_{VH}$ | $I_{HH}$ |
|---|---|---|---|---|
| Rotational diffusion | $P^2$ | 1 | 1 | 1 |
| Collision-induced | $Q^2$ | 1 | 1 | 1 |
| Transverse | $R^2$ | 1 | 1/2 | 1/2 |
| Longitudinal | 0 | 0 | 1/2 | 1/2 |

tion dependence, as proposed in Ref. 6. This polarization dependence is illustrated in Table I which shows that the ratio $I_{HV}/I_{VH}=1$ for local modes, 2 for transverse polar modes or 0 for longitudinal polar modes. The parameters $P^2$, $Q^2$, and $R^2$ depend on molecular structure, but the relations between the HV, VH, and HH intensities for each mode do not.

The peak HRS signal was typically 20 counts/s (cps) for VV polarization and $<1$ cps for VH (dead-time corrections[10,12] were $<1\%$). $D_2O$ was chosen as the sample liquid instead of $H_2O$ because thermal defocusing[10,13] of the 1064 nm laser beam reduced the signal from $H_2O$ by a factor of 3. Gated photon counting detection was used, giving a typical gated photomultiplier dark count rate of $2\times10^{-4}$ cps, which was negligible even for the weakest HRS spectra. There was no detectable contribution to the HRS signal due to scattering from the residual dust in the samples. Most of the spectra were acquired with 1.25 $cm^{-1}$ spectral resolution [full width at half maximum intensity (FWHM)]. The spectral response function of the instrument was the convolution of the spectrometer function (0.80 $cm^{-1}$ FWHM triangle) and the laser spectrum (0.95 $cm^{-1}$ FWHM Gaussian). The spectral response function was measured by scanning the spectrum of the laser beam after it had been frequency doubled with a KTP crystal and reflected from a scatter plate at the sample position.

The directions and polarizations of the incident and scattered beams were aligned along mutually orthogonal axes, and the center of the scattered beam was placed on the optical axis of the spectrometer, constructing the nominal scattering geometry with angular errors $<0.2°$. The linear polarization ratio for the laser beam after the LCVWP is $>5000:1$ for both zero and half-wave settings, and the transmitted laser intensity differed $<0.1\%$ for the two settings. The extinction ratio of the analyzing polarizer is $8\times10^{-5}$. The wavefront deflection and distortion by the plane parallel polarizer surfaces is $<1/30$ wave, such that the beam deflection when the polarizer is flipped from V to H polarization is negligible. Since the spectrometer slits are narrow to achieve high resolution, small displacements of the image of the source across the slit due to a wedge in the polarizer would result in systematic errors in the measured polarization ratios. Étalon fringes from the plane parallel polarizer are not a problem because the polarizer is placed in the convergent beam focused on the entrance slit of the spectrometer. The spectrometer response ratio for V and H polarized light is about 4.6 at $\lambda=532$ nm. This reduces the VH signal compared to VV and HV, so that the VH data is usually the limiting factor in the signal to noise ratio for the overall measurement. A quartz wedge polarization scrambler was not used since the strong, coarse polarization modulation it introduces can result in large systematic errors in this experiment. The aperture stop for the detection system is a rectangular aperture at the position of the relay mirror coupling the tandem monochromators of the Jobin-Yvon Ramanor U 1000 spectrometer. The physical aperture stop in the spectrometer defines an $f/11.4\times f/17.5$ rectangular acceptance cone at the entrance slit, which is imaged to a rectangular collection aperture inside the sample with angular size $\Delta\theta=\pm9.9°$ parallel and $\Delta\psi=\pm6.6°$ perpendicular to the scattering plane, respectively. A large collection aperture is necessary due to the weakness of the HRS, but collection of light over this large angular range effectively mixes polarization components of the scattered light. Corrections for finite collection angle are calculated using the results in Ref. 7, and were tested using measurements of the strongly polarized Rayleigh scatter from liquid $CCl_4$. The spectrometer polarization response was calibrated using unpolarized light from a tungsten lamp and integrating sphere, and also using two photon fluorescence (2PF) from Rhodamine 590 dye solution with an H polarized laser beam incident. Experimental tests for biases in the polarization response of the LCVWP and the analyzing polarizer, and deviations from the nominal scattering angles and polarizations, were made using tungsten lamp, 2PF and Rayleigh scattering light sources.

## III. RESULTS AND ANALYSIS

The HRS measurements for liquid $D_2O$ over a 10 $cm^{-1}$ spectral range at temperatures between 22.8 and 80.0 °C are shown in Fig. 1. HRS spectra measured for $H_2O$ (this work, not shown) are similar. The data have been corrected for dead time and spectrometer polarization response, and the VV, HV, and VH spectra at each temperature have been placed on a common intensity scale using the HV spectrum as the reference. Intensity is plotted as a function of frequency shift from the second harmonic frequency of the laser (the Stokes side of the spectrum corresponds to negative frequency shift). The error bars on the data points include only counting statistics and are largest for the VH spectra. Although the VV intensity is much higher, the VV and HV spectra at each temperature are similar in shape and width, and to a good first approximation can be represented by simple Lorentzian functions with width about 2 $cm^{-1}$ FWHM. HRS from uncorrelated orientational fluctuations of the molecules is expected to produce identical HV and VH spectra, but this is evidently not the case. The VH spectrum is narrower than the HV spectrum at all temperatures, and has higher peak intensity.

The relative intensities and shapes of the spectra for different polarizations can be compared in more detail by examining the intensity ratios. Figure 2 shows the ratio of intensities for the VV and HV spectra. The ratio decreases away from line center, particularly at low temperature where the central peak is narrow, indicating that there is an additional broad, more weakly polarized contribution to the HRS spectrum. Figure 3 shows the ratio of intensities for the HV and VH spectra. At every temperature the HV/VH intensity ratio is significantly different from the constant value equal

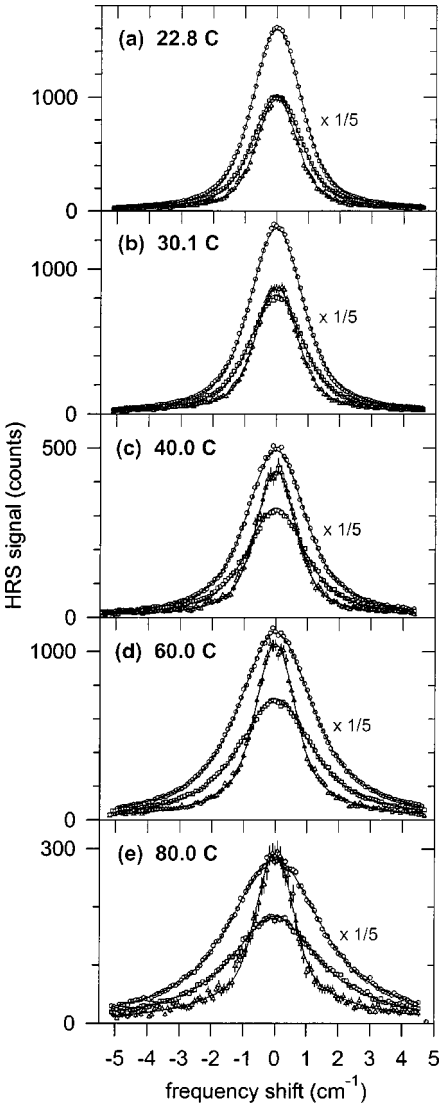


FIG. 1. HRS spectral intensities measured in the VV (circles), HV (squares), and VH (triangles) polarization geometries for liquid $D_2O$ at five temperatures. Note that $I_{VV}/5$ is plotted to facilitate comparison with $I_{HV}$ and $I_{VH}$. The solid curves are obtained by a weighted least squares fit to the data (see text). The spectral resolution is 1.25 cm$^{-1}$ FWHM.

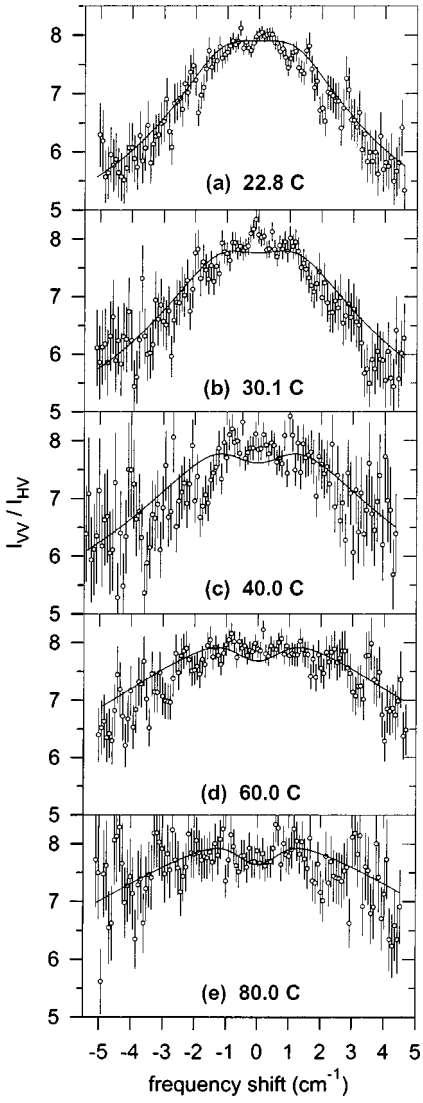


FIG. 2. Polarization ratios $I_{VV}/I_{HV}$ obtained from the HRS spectral intensity data in Fig. 1 for $D_2O$ at five temperatures. The solid curves are the ratios of the fitted VV and HV spectral intensities from Fig. 1.

to 1 expected for local modes, and the nonmonotonic variation of the ratio as the frequency shifts away from line center suggests that at least three spectral components with different polarization dependence and width are present.

The HRS spectrum was scanned over a wider frequency range at lower spectral resolution to investigate the nature of the background underlying the narrow peaks in Fig. 1. The spectrum obtained with 24 cm$^{-1}$ spectral slit width at $T=60\,^{\circ}\mathrm{C}$ is shown in Fig. 4. One sees an instrumentally broadened central peak on top of broad exponential wings. The VH spectrum nearly coincides with the HV spectrum at low frequency, but lies above it in the wings. The VV/HV polarization ratio switches from about 7.4 at line center to about 2.7 in the wings. The HV/VH polarization ratio is about 1.03 at line center and decreases in the wings due to the excess VH intensity there. The broad exponential wings seen in the low resolution spectra in Fig. 4 will appear as a nearly flat background in the higher resolution spectra in Fig. 1.

The fitted curves shown in Figs. 1–4 are the sum of several overlapping spectral components. The narrow peaks visible in Fig. 1 are assumed to be the sum of three Lorentzians with distinct polarization dependence (components 1, 2, and 3). The broad background underlying the peaks in Fig. 1 and visible Fig. 4 is represented as the sum of a centered Lorentzian $(1+(\nu/\nu_4)^2)^{-1}$ and an exponential profile $\exp(-|\nu/\nu_5|)$ (components 4 and 5), and a pair of Lorentzian peaks at $\pm 175$ cm$^{-1}$ with width 230 cm$^{-1}$ FWHM (component 6). The adjustable parameters are the intensity, width, and polarization ratio for each component. Information from other sources suggests the form of the fit function, and is used to constrain the values of some of the parameters. The calculated spectrum is multiplied by a Boltzmann factor $\exp(-hc\nu/2kT)$ to account for the Stokes/anti-Stokes asymmetry, convolved with the instrument spectral response function, and adjusted for finite collection angle effects. This syn-

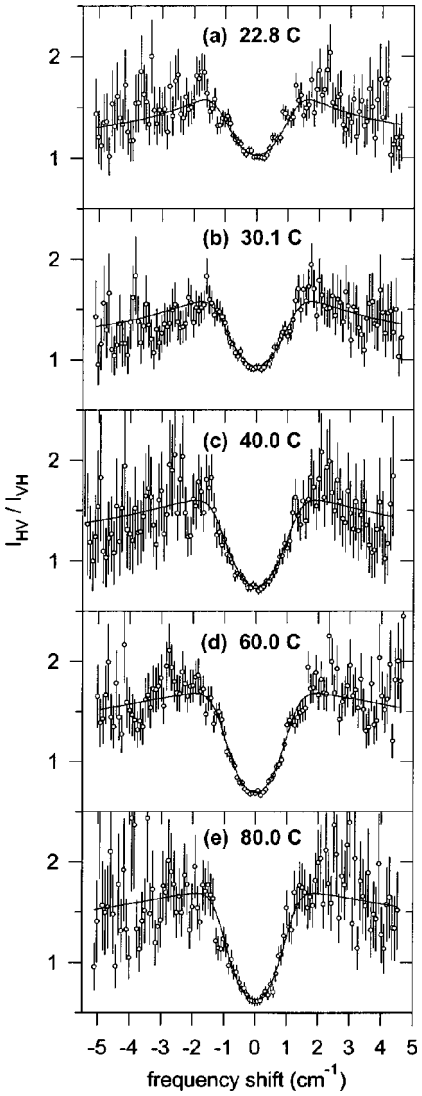


FIG. 3. Polarization ratios $I_{HV}/I_{VH}$ obtained from the HRS spectral intensity data in Fig. 1 for $D_2O$ at five temperatures. The solid curves are the ratios of the fitted HV and VH spectral intensities from Fig. 1.

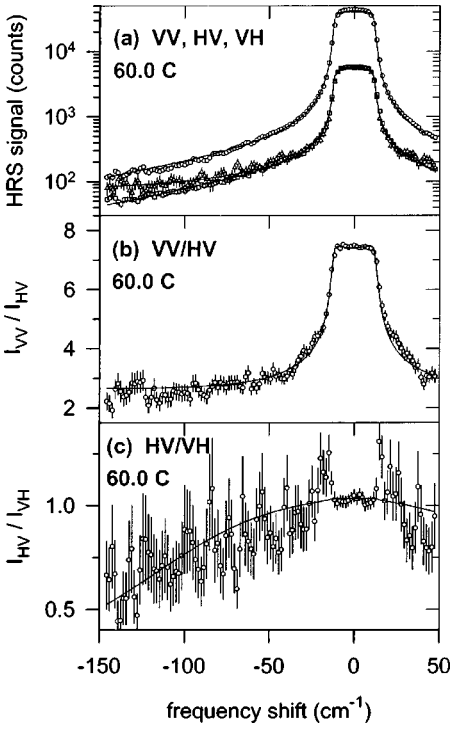


FIG. 4. (a) HRS spectral intensities measured in the VV (circles), HV (squares), and VH (triangles) polarization geometries for liquid $D_2O$ at 60 °C. The solid curves are obtained by a weighted least squares fit to the data (see text). The spectral resolution is 24 $cm^{-1}$ FWHM. (b) Polarization ratio $I_{VV}/I_{HV}$ obtained from the HRS spectral intensity data in (a). The solid curve is the ratio of the fitted VV and HV spectral intensities. (c) Polarization ratio $I_{HV}/I_{VH}$ obtained from the HRS spectral intensity data in (a). The solid curve is the ratio of the fitted HV and VH spectral intensities.

thetic spectrum can be directly compared with the measured spectrum.

Finite angle corrections are included at the curve fitting stage since the correction terms are a function of the spectral components in the fit. Expressions for the measured intensities including finite angle effects are[7]

$$I_{VV}=[1-(1-P^{-2})a]P^2A_1F_1+[1-2.28a]R^2A_2F_2 +[12a]A_3F_3 +[1-(1-Q^{-2})a]Q^2A_4F_4, \quad (1)$$

$$I_{HV}=[1+(P^2-1)a]A_1F_1+[1+7.5a]A_2F_2 +[12a]A_3F_3+[1+(Q^2-1)a]A_4F_4, \quad (2)$$

$$I_{VH}=A_1F_1+[1+a](1/2)A_2F_2+A_3F_3+A_4F_4, \quad (3)$$

$$I_{HH}=[1+(P^2-1)b]A_1F_1+[1+a+8b](1/2)A_2F_2 +[1+8b]A_3F_3+[1+(Q^2-1)b]A_4F_4, \quad (4)$$

where $a=\Delta\psi^2/3=4.34\times10^{-3}$, $b=\Delta\theta^2/3=9.93\times10^{-3}$, and $R^2\approx9$ is assumed. The four spectral functions $F_i$ with distinct polarization dependencies are constructed from the six components described above, and are normalized to unit intensity at $\nu=0$. The polarization dependence for $F_1$ and $F_4$ corresponds to local modes, while that for $F_2$ and $F_3$ corresponds to transverse and longitudinal polar modes, respectively. These expressions are applied, with $P^2$, $R^2$, $Q^2$, $A_i$, and $\nu_i$ (in the functions $F_i$) as adjustable parameters, to fit the VV, HV, and VH spectra simultaneously.

The weak, broad HRS background in Fig. 1 is assumed to be collision-induced light scattering due to the dipole-induced dipole (DID) mechanism, with the same spectral profile as observed for the depolarized Raman spectrum of water.[14] The fit to the data at $T=60$ °C in Fig. 4 is used to determine the polarization ratio for the HRS background. A simplified fitting procedure was used. The three narrow components were treated as a single Lorentzian with width 2.4 $cm^{-1}$, the broad Lorentzian width was set to $2\nu_4=17.6$ $cm^{-1}$, the peak intensity ratio for the exponential and broad Lorentzian components was set to $I_5/I_4=0.30$, the instrument function was approximated as a 24 $cm^{-1}$ wide rectangle, and the VV, HV, and VH spectra were fit separately. The ratio of VV and HV intensities (assuming local mode finite angle corrections) is 8.46 for the narrow components and 2.32 for the broad components. The exponential

TABLE II. Parameters obtained by a weighted least squares fit of Eqs. (1)–(4) to the VV, HV, and VH HRS spectra in Fig. 1. The Lorentzian functions $L_i(\nu,\nu_i)=(1+(\nu/\nu_i)^2)^{-1}$, specified by the width parameters $\nu_1$, $\nu_2$, and $\nu_3$, are convolved with the instrument response function and normalized to generate the functions $F_1$, $F_2$, and $F_3$. The convolved, normalized DID profile $F_4$ is described in the text and specified by the parameters in Table III. The parameters $A_1$, $A_2$, $A_3$, and $A_4$ are the intensities of the local, transverse, and longitudinal, and DID contributions to the HRS spectrum, respectively. The common values $P^2=8.3$, $R^2=8.5$, and $Q^2=2.32$ are used for all five fits. The formal error bars on the widths are $<0.1$ cm$^{-1}$.

| $T$ (°C) | $2\nu_1$ (cm$^{-1}$) | $2\nu_2$ (cm$^{-1}$) | $2\nu_3$ (cm$^{-1}$) | $A_1$ (counts) | $A_2$ (counts) | $A_3$ (counts) | $A_4$ (counts) |
|---|---|---|---|---|---|---|---|
| 22.8 | 1.2 | 1.0 | 0.0 | 119.4 | 822.5 | 431.2 | 22.1 |
| 30.1 | 1.1 | 1.3 | 0.0 | 198.3 | 562.5 | 378.1 | 19.4 |
| 40.0 | 1.2 | 1.7 | 0.0 | 82.8 | 210.3 | 238.4 | 7.0 |
| 60.0 | 2.0 | 2.4 | 0.0 | 123.0 | 531.4 | 641.9 | 14.7 |
| 80.0 | 3.3 | 3.1 | 0.0 | 24.6 | 140.5 | 191.2 | 4.6 |

width parameter is $\nu_5=70$ cm$^{-1}$ (constrained to be the same for all three spectra). Only the VH fit includes the Lorentzian peaks at $\pm 175$ cm$^{-1}$. The relative intensities at $\nu=0$ cm$^{-1}$ are 88% and 12% for the narrow and wide components scanned with 24 cm$^{-1}$ spectral slit width, but the contribution of the wide component will fall to about 3% when the resolution is 1 cm$^{-1}$.

The fitted curves shown in Fig. 1 are linear combinations of four spectral functions $F_i$ with polarization dependence given by Eqs. (1)–(4). The first three functions are Lorentzians convolved with the instrument function, and $F_4$ is the DID spectral profile of the form $[I_4/(1+(\nu/\nu_4)^2)+I_5\exp(-|\nu/\nu_5|)]\times\exp(-hc\nu/2kT)$, with $\nu_5=70$ cm$^{-1}$ and polarization ratio $Q^2=2.32$, convolved with the instrument function. The curves shown in Figs. 2 and 3 are ratios of the fitted intensity functions shown in Fig. 1. The parameters obtained from simultaneous fits to the VV, HV, and VH spectra at each temperature are given in Table II, and the parameters describing the DID spectral profile at each temperature are given in Table III. The values of the polarization parameters $P^2$, $R^2$, and $Q^2$ are constrained to be the same at all temperatures. Normalized relative peak and integrated intensities of four spectral functions at each temperature are given in Table IV. The fitted functions adequately represent the data at all temperatures, and the value $\chi^2=1656$ obtained for the simultaneous fit to all the data in Fig. 1 (with error bars determined by counting statistics alone) is in agreement with $\chi^2=1711\pm 58$ expected for a good fit to 1748 data points with 37 adjustable parameters. As a further check, the HH and VH spectra were measured at $T=60$ °C to obtain the spectral intensity ratio data shown in Fig. 5. The curve is the prediction based on the fits to the VV, HV, and VH spectra at the same temperature. There are no adjustable parameters and the predicted curve is in good agreement with the data.

## IV. DISCUSSION AND CONCLUSION

Collective modes of molecular reorientation in $D_2O$ are clearly indicated by the deviations from the HRS polarization ratio $I_{HV}/I_{VH}=1$ shown in Fig. 3. The ratio $I_{HV}/I_{VH}=1$, 2 or 0 for pure local, transverse, or longitudinal modes, respectively, so deviations from 1 are the signature of collective mode contributions.[6,7] The observed difference between the HV and VH spectra for water is the principal result of this work.

The present results are consistent with the few previous observations. Maker measured the width and polarization of the hyper-Rayleigh peak for water in his pioneering work on the HRS spectra of liquids.[15] He observed a Lorentzian profile for the VV spectrum of $H_2O$, and his values for the deconvolved width (FWHM) are $1.2\pm 0.1$ cm$^{-1}$ at 25 °C and $2.8\pm 0.5$ cm$^{-1}$ at 60 °C, in close agreement with the results given in Table II for $D_2O$. His value $8.6\pm 0.6$ at 25 °C for the polarization ratio is consistent with the results in Fig. 2 for $D_2O$. Deviations from $I_{HV}/I_{VH}=1$ for water can have escaped notice in Maker's work since the room temperature value of the ratio is close to 1 when observed at $\nu=0$ cm$^{-1}$ with spectral resolution about 1 cm$^{-1}$. This occurs because the true spectral width of the HV spectrum decreases to about 1 cm$^{-1}$ at 20 °C so that the instrumentally broadened HV spectrum is only slightly wider than the instrumentally broadened VH spectrum; and since the HV integrated intensity is also slightly larger than the VH integrated intensity the peak intensities end up nearly the same. The observed polarization ratio $I_{HV}/I_{VH}$ at $\nu=0$ cm$^{-1}$ would be close to 0 at all temperatures if all spectra were fully resolved. Conversely, this ratio will be close to 1 at all temperatures when observed at low spectral resolution, since the integrated intensity of the rotational HRS spectrum at all temperatures is about 10% larger for HV as compared to VH (see Table IV and Fig. 4). The only other measurements of the HRS polarization ratios reported for water are also consistent with the present results (systematic errors as large as 20% due to the polarization scrambler are now believed to have occurred in that work).[6]

TABLE III. Parameters describing the DID HRS spectrum, based on Ref. 14.

| $T$ (°C) | $2\nu_4$ (cm$^{-1}$) | $I_5/I_4$ |
|---|---|---|
| 22.8 | 10.0 | 0.17 |
| 30.1 | 11.4 | 0.19 |
| 40.0 | 13.4 | 0.23 |
| 60.0 | 17.6 | 0.30 |
| 80.0 | 21.8 | 0.37 |

TABLE IV. Normalized relative peak and integrated intensities of spectral components. $A_n^*=A_n/(A_1+A_2)$ and similarly for $B_n^*$, where $A_n$ comes from Table II and $B_n$ are the integrated intensities for the corresponding spectral components. The $A_n$ values vary with spectral resolution, but $B_n$ are independent of resolution used.

| $T$ (°C) | $A_1^*$ | $A_2^*$ | $A_3^*$ | $A_4^*$ | $B_1^*$ | $B_2^*$ | $B_3^*$ | $B_4^*$ |
|---|---|---|---|---|---|---|---|---|
| 22.8 | 0.13 | 0.87 | 0.46 | 0.023 | 0.14 | 0.86 | 0.26 | 5.3 |
| 30.1 | 0.26 | 0.74 | 0.50 | 0.025 | 0.25 | 0.76 | 0.25 | 5.8 |
| 40.0 | 0.28 | 0.72 | 0.70 | 0.024 | 0.25 | 0.76 | 0.36 | 5.5 |
| 60.0 | 0.19 | 0.81 | 0.98 | 0.022 | 0.17 | 0.83 | 0.34 | 5.0 |
| 80.0 | 0.15 | 0.85 | 1.16 | 0.028 | 0.16 | 0.85 | 0.33 | 6.0 |
| Average ±S.D. | 0.20 ±0.06 | 0.80 ±0.06 | 0.76 ±0.27 | 0.024 ±0.002 | 0.19 ±0.05 | 0.81 ±0.05 | 0.31 ±0.05 | 5.5 ±0.4 |

The local and transverse mode spectra obtained from the fit to the data in Fig. 1 have almost the same width, so the values of the parameters $P^2$ and $R^2$ are strongly correlated and a plot of $\chi^2$ as a function of $P^2$ and $R^2$ shows a long, narrow valley. The contour extending from $(P^2,\ R^2)=(5.8,\ 9.2)$ to (13, 7.4) encloses $\chi^2$ values in the expected range for a good fit ($\chi^2=1711\pm58$), and the global minimum is $\chi^2=1656$ at $(P^2,\ R^2)=(8.3,\ 8.5)$. The fit to the data is consistent with a wide range for the parameters $P^2$ and $R^2$, so additional information has been used to select the best estimates. The first constraint is that the value for $R^2$ must be close to the limiting value $R^2=9$ that is required when Kleinman symmetry holds.[5] Kleinman symmetry is the invariance of the hyperpolarizability tensor under permutation of the spatial indices, which is exact in the static limit, and is a good approximation when all field frequencies are far from resonance.[16] The deviations from Kleinman symmetry are expected to be small since the applied field frequencies are far from resonance. The second constraint is that the value for $P^2$ must be consistent with the values of the components of the first hyperpolarizability tensor, $\beta_{\alpha\beta\gamma}$, obtained from *ab initio* quantum chemical calculations and nonlinear optical experiments.

The parameter $P^2=I_{VV}/V_{VH}=\langle\beta_{ZZZ}^2\rangle/\langle\beta_{XZZ}^2\rangle$, where $\beta_{ZZZ}$ is the space-fixed $ZZZ$ component of the $\beta$ tensor and $\langle\ \rangle$ denotes the ensemble average. In the case that molecular orientations are uncorrelated and molecular interactions are negligible, the ensemble average reduces to the isotropic average for a single molecule, and $P^2$ can be expressed in terms of the molecule-fixed components of the $\beta$ tensor using Cartesian[17] or irreducible spherical[15,18–21] tensor calculations. For the water molecule, which has $C_{2v}$ symmetry, the expressions are[15,16]

$$\langle\beta_{ZZZ}^2\rangle=(15\times35)^{-1}[7(3A+B+C)^2+3(2A-B-C)^2+5(B-C)^2], \tag{5}$$

$$\langle\beta_{XZZ}^2\rangle=(9\times15\times35)^{-1}[7(3A+B+C)^2+18(2A-B-C)^2+30(B-C)^2-35(3A+B+C)(D+E)+\tfrac{174}{4}(D+E)^2+\tfrac{105}{4}(D-E)^2], \tag{6}$$

where $A=\beta_{333}$, $B=2\beta_{113}+\beta_{311}$, $C=2\beta_{223}+\beta_{322}$, $D=2(\beta_{113}-\beta_{311})$, and $E=2(\beta_{223}-\beta_{322})$. The index 3 $(=z)$ refers to the molecular two-fold axis, 2 $(=y)$ is the axis perpendicular to the molecular plane, and 1 $(=x)$ is the axis perpendicular to the other two. (The expression for $\langle\beta_{XZZ}^2\rangle$ in Appendix B of Bersohn *et al.*[17] has the parentheses missing from the term 2/105 $(s_{15}^2+s_{24}^2)$, and the entry for $zzz$ and $[ss,3]$ in Table II of Maker[15] should have a + sign, as previously noted in Refs. 18 and 19.) When Kleinman symmetry holds $\beta_{113}=\beta_{311}$, $\beta_{223}=\beta_{322}$, $D=E=0$, and $9\geqslant P^2\geqslant3/2$, but when Kleinman symmetry is broken $P^2>9$ can occur through the term $-35(3A+B+C)(D+E)$.

The *ab initio* results used to determine $P^2$ for water are shown in Table V. The $\beta$ values which pertain to the experiment are obtained by adding dispersion and vibration corrections to the static, pure electronic $\beta^e$ (nuclei fixed at the equilibrium positions). The calculation of Maroulis[22] most thoroughly investigates the effects of basis set and electron correlation, and his result has been taken as the best static estimate of $\beta^e$. As an indication of the degree of agreement of recent calculations,[22–25] one may compare the calculated values of $\beta_\parallel=1/5\ \Sigma_i\ (\beta_{3ii}+\beta_{i3i}+\beta_{ii3})=(3A+B+C)/5$, the mean value of $\beta$ in the direction of the molecular dipole moment. Multiconfiguration self-consistent-field (MCSCF) calculations give static $\beta_\parallel^e$ values (in atomic units) ranging from −15.25 a.u. (Ref. 23) to −19.4 a.u.,[24] with corresponding $P^2$ values 7.4 and 7.6, whereas the highest level coupled cluster calculations (CCSD(T)) give static $\beta_\parallel^e$ values ranging from −17.51 a.u. (Ref. 22) to −18.0 a.u.,[25] with corresponding $P^2$ values 7.7 and 7.6. The $P^2$ values depend on ratios of

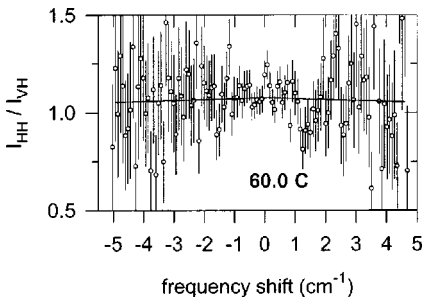


FIG. 5. Polarization ratio $I_{HH}/I_{VH}$ obtained from HRS spectral intensity data for $D_2O$ at 60 °C with 1.25 $cm^{-1}$ resolution. The solid curve is predicted from the fits to the VV, HV, and VH spectra.

TABLE V. *Ab initio* results for $\beta$ and $P^2$ of gas-phase water at $\omega=0.0428$ a.u. (corresponding to laser wavelength $\lambda=1064$ nm). All values are given in atomic units (a.u.).

| | | | $\beta^{\mathrm{ZPVA}}(0;0,0)$[c] | | $\beta^{v}(-2\omega;\omega,\omega)$[c] | | $\beta(-2\omega;\omega,\omega)$ | |
|---|---|---|---|---|---|---|---|---|
| | $\beta^{e}(0;0,0)$[a] | $\Delta\beta^{e}$ [b] | $H_2O$ | $D_2O$ | $H_2O$ | $D_2O$ | $H_2O$ | $D_2O$ |
| $\beta_{113}$ | −9.80 | −0.50 | −1.069 | −0.756 | −0.435 | −0.291 | −11.80 | −11.35 |
| $\beta_{311}$ | −9.80 | −0.56 | −1.069 | −0.756 | −0.575 | −0.384 | −12.00 | −11.50 |
| $\beta_{223}$ | −5.61 | −1.16 | +0.145 | +0.103 | −0.038 | −0.025 | −6.63 | −6.69 |
| $\beta_{322}$ | −5.61 | −0.28 | +0.145 | +0.103 | −0.008 | −0.005 | −5.75 | −5.79 |
| $\beta_{333}$ | −13.77 | −1.01 | −0.655 | −0.463 | −0.365 | −0.244 | −15.80 | −15.49 |
| $\beta_{\parallel}$ | −17.51 | | | | | | −20.42 | −19.97 |
| $\langle\beta^2_{ZZZ}\rangle$ | 105.68 | | | | | | 142.87 | 136.04 |
| $\langle\beta^2_{XZZ}\rangle$ | 13.69 | | | | | | 20.22 | 19.11 |
| $P^2$ | 7.72 | | | | | | 7.06 | 7.12 |

[a]Reference 22.
[b]References 23 and 24.
[c]Reference 26.

$\beta$ components and appear to be more reliable than the absolute size of the $\beta$ components.

The dispersion correction to static $\beta^e$ was obtained by scaling $\Delta\beta^e=[\beta^e(-2\omega;\omega,\omega)-\beta^e(0;0,0)]$ calculated at $\omega=0.0656$ a.u. to $\omega=0.0428$ a.u. assuming $\omega^2$ dependence. The results from the two MCSCF calculations[23,24] were averaged (note that the choice of axes varies from one calculation to the next). Deviations from Kleinman symmetry at $\omega=0.0656$ a.u. are such that $P^2>9$ for $\beta^e$. The zero point vibration averaging (ZPVA) and pure vibration ($v$) corrections come from calculations at the MP2 level of electron correlation by Bishop *et al.*[26] The $\beta^{\mathrm{ZPVA}}$ result for $D_2O$ is obtained from the $H_2O$ result assuming $M^{-1/2}$ scaling, where $M$ is the reduced mass of the vibrating atoms. The pure vibration contribution $\beta^v$ at $\omega=0.0428$ a.u. is obtained from the result at 0.070 a.u. assuming $\nu_0/(\nu^2-\nu_0^2)$ frequency dependence, where $\nu_0\propto M^{-1/2}$ and $\nu_0=3000$ cm$^{-1}$ for $H_2O$. The final results for $\beta_{\parallel}$ in Table V are in fair agreement with $-19.2\pm0.9$ and $-17.8\pm1.2$ a.u. measured for $H_2O$ and $D_2O$ by gas-phase electric-field-induced second harmonic generation experiments at this wavelength,[27] and the final results for $P^2$ are expected to be more accurate than the results for $\beta_{\parallel}$.

The value $P^2=7.1$ for $D_2O$ in Table V neglects short range orientation correlations and interactions. The effects of condensation on $\beta$ are not small. A recent calculation at the CCSD(T) level by Maroulis[28] finds that static $\beta_{\parallel}$ changes from $-17.51$ a.u. for the monomer $H_2O$ to $-6.5$ a.u. for the dimer $(H_2O)_2$. Experimentally it is determined that $\beta_{\parallel}$ for water changes sign going from the gas phase to the liquid.[27,29] Calculations can account for this sign change when nearest neighbor molecules are explicitly included.[30,31] An estimate for $P^2$ of liquid water can be obtained from a recent calculation[31] which treats $\beta$ for a single solute water molecule by MCSCF, in the presence of 127 surrounding water molecules which are treated by molecular mechanics, and whose positions are determined by a molecular dynamics simulation. The calculated static value of $\beta_{\parallel}$ goes from $-14.4$ a.u. in the gas phase to $+14.2$ a.u. in the liquid, and the value of $P^2$ goes from 7.2 to 6.7.[31] An alternative approach[32] to the calculation of $\beta$ in liquid water starts with a classical molecular dynamics simulation to estimate the mean field and field gradient at the position of a water molecule, and then uses an *ab initio* finite field calculation to obtain multipole moments, polarizabilities, hyperpolarizabilities, and field gradient polarizabilities for a single water molecule with the mean field and field gradient of liquid water applied as the background field. This calculation shows that the intense local field $F$ at the site of a water molecule increases $\beta$ by an increment $\gamma F$ which is twice as large as the magnitude of $\beta$ for the isolated molecule. The static value of $\beta_{\parallel}$ calculated at the MP4-SDTQ level goes from $-19.3$ a.u. in the gas phase to $+28.9$ a.u. in the liquid, and the value of $P^2$ goes from 8.2 to 8.5.[32] The change in $P^2$ for a water molecule moved from gas to liquid is sensitive to the calculated value of the local field distorting the water molecule in the liquid, and for example, using the local field and gradient corresponding to ice gives $P^2=5.6$ instead of 8.5.[32] Based on these calculations our estimate of the change in the value of $P^2$ from gas to liquid to $0.0\pm0.5$.[31,32]

Orientation correlation of neighboring molecules directly influences the intensity and polarization of the HRS. To estimate this effect for water it is most convenient to express the hyperpolarizability tensor as the sum of irreducible spherical tensors. In the static limit one has $\boldsymbol{\beta}=\boldsymbol{\beta}^{(1)}+\boldsymbol{\beta}^{(3)}$, where $|\beta^{(1)}|^2=(5/3)(\beta_{\parallel})^2$ and $|\beta^{(3)}|^2=(1/10)(2A-B-C)^2+(1/6)(B-C)^2$, and for water $|\beta^{(1)}|^2/|\beta^{(3)}|^2\approx5$. The transformation of $\boldsymbol{\beta}^{(1)}$ under rotations is the same as for the molecular dipole. One can show that the effect of short range orientation correlation on the first rank contribution of the HRS intensity is to multiply $|\beta^{(1)}|^2$ by Kirkwood's correlation parameter $g=1+\Sigma_j N_j\langle\cos\gamma_j\rangle$, where $\gamma$ is the angle between the axis of a neighboring molecule and that of the central molecule, and $N_j$ is the number of molecules in the $j$th coordination shell.[8] Ignoring the effect of orientation correlation on the smaller third rank contribution, one has $P^2=9(7g|\beta^{(1)}|^2+2|\beta^{(3)}|^2)/(7g|\beta^{(1)}|^2+12|\beta^{(3)}|^2)$. Taking $g\approx2.5$ for liquid water[8] one calculates an increase from 7.1 to 8.1 for $P^2$. Adding the effects of the liquid environment and orientation correlation to the gas phase value gives $P^2=7.1+0.0+1.0=8.1$, insignificantly different from the value 8.3 for the experimental best fit.

Since the experimentally determined best fit parameters $P^2=8.3$ and $R^2=8.5$ are consistent with the theoretically expected value for $P^2$ and $R^2$, the experimental best fit parameter values have been used for the curves fitted to the spectral peaks in Fig. 1.

The broad underlying spectral component in Fig. 1, with polarization ratio $Q^2$, is analogous to a component previously observed in the depolarized Raman (or Rayleigh) spectrum of water. The depolarized Raman spectrum measured at high resolution[14] shows no component narrower than 10 $cm^{-1}$, and is consistent with collision-induced light scattering (CILS) mediated by the dipole-induced dipole (DID) mechanism, with no significant contribution from the allowed rotational spectrum. There will be a DID HRS spectrum with the same profile as the DID Raman spectrum. The depolarized Raman spectrum in Ref. 14 was represented by the sum of two Lorentzian peaks centered at 0 $cm^{-1}$, and while the relative intensity of the two components at 0 $cm^{-1}$ is well determined, the spectral range of the data is too narrow ($\pm 50$ $cm^{-1}$) to exclude an exponential rather than a Lorentzian profile for the broadest component of the depolarized spectrum. Since the spectral wing observed in collision-induced light scattering is typically exponential, we have expressed the DID spectrum as the sum of the narrow Lorentzian given in Ref. 14, and an exponential with peak intensity the same as the wide Lorentzian in Ref. 14 and with slope given by the fit to the data in Fig. 4. The polarization ratio of the binary DID HRS spectrum can be calculated using the expressions derived by Keilich *et al.*[33] *Ab initio* values for the tensor components of $\boldsymbol{\alpha}$ and $\boldsymbol{\beta}$ for $D_2O$ in the gas phase[22] were used to evaluate Eqs. (26) and (D1)–(D7) of Ref. 33 (neglecting the very small anisotropy of $\alpha$). Note that the right-hand side of Eq. (D6) in Ref. 33 should be multiplied by a minus sign so that it gives results consistent with Eq. (69) in Ref. 33. The calculated polarization ratio is $I_{VV}/I_{HV}=2.34$, in close agreement with the observed value 2.32, supporting the identification of the HRS background as DID CILS. Note that the integrated intensity of the weak but very broad DID spectrum is actually larger than that of the allowed HRS molecular reorientation spectrum (see Table IV).

Previous lower resolution Raman spectroscopic measurements of the polarized and depolarized Raman spectra of water over a wide frequency range identify three features at frequencies below 300 $cm^{-1}$.[34–37] Those investigations found two peaks resting on a broad sloping background extending several hundred $cm^{-1}$. The sloping background is the DID CILS spectrum. The peaks in liquid water, at 55 $cm^{-1}$ with width 60 $cm^{-1}$ FWHM, and at 175 $cm^{-1}$ with width 230 $cm^{-1}$ FWHM, correspond to the TA shear and LA dilation phonon modes at about the same frequency in ice.[34] No peak at 55 $cm^{-1}$ appears in the HRS spectra of Fig. 4, but the VH spectrum shows a contribution consistent with a broad peak at 175 $cm^{-1}$. As expected for a LA mode, there is no corresponding contribution to the VV or HV spectra.

The strongest components of the HRS spectrum have no counterpart in the Raman spectrum, and vice versa. The polarized Raman spectrum measured at high resolution[14,38] is dominated by the Brillouin doublet, a pair of narrow peaks at $\pm 6$ GHz (the Rayleigh line is weak in water). The source of this spectrum is density fluctuations, principally sound waves. The Rayleigh–Brillouin triplet is absent from the HRS spectrum. Instead the VV and HV HRS spectra show a relatively wide Lorentzian peak due to orientation fluctuations of the molecules, and the VH HRS spectrum shows an instrumentally broadened peak. The polarization dependence of these two contributions to the HRS spectrum indicates that they are due to polar TA and LA orientation modes, respectively. Contributions from these collective modes are forbidden in the linear Raman spectrum. No information about molecular rotation is contained in the low frequency Raman spectrum of liquid water since even the allowed local orientation-diffusion Raman spectrum of water is too weak to observe because of the nearly isotropic $\boldsymbol{\alpha}$ tensor for the water molecule.

The novel features in the HRS spectra are the collective polar orientation modes. The spectrally resolved TA mode shows only a single peak centered at 0 $cm^{-1}$, indicating that the mode is highly damped. The spatial correlation length cannot be unambiguously determined from the HRS spectrum at a single scattering angle, but decay of the excitation within a fraction of a cycle of oscillation suggests that the correlation length is also small. The dependence of the HRS intensity on direction of the recoil momentum $h\Delta K/2\pi$, as well as the polarization of the incident and scattered fields, differentiates this mode from a point excitation of a single molecule followed by orientation diffusion. Momentum conservation for HRS by a single water molecule requires $3\times10^{-6}$ $cm^{-1}$ recoil energy, which is negligible compared to the rotational energy scale, so recoil and reorientation can be essentially uncoupled. For a wavelike excitation the energy per unit of momentum carried is much lager ($10^5\times$larger for an acoustic phonon) because of the coordinated motion of the molecules, and the recoil direction and the reorientation direction will be strongly coupled. The molecular motion for the polar TA mode may be coupled reorientation and shear flow. Such coupling between shear flow and molecular orientation gives rise to line shape distortions seen in the depolarized Rayleigh scattering spectrum.[1–3,39]

The LA mode is spectrally unresolved. The deconvolved width is consistent with zero, but a width as large as 0.3 $cm^{-1}$ also gives a fit with $\chi^2$ within the expected range of $\chi^2$ values for a good fit. The HRS spectrum must be resolved to determine the nature of this mode. One possibility is that the VH HRS peak is a doublet with the same splitting as the Brillouin doublet, and a possible interpretation would be that there is a coupling between density fluctuations in the sound wave and longitudinal polarization of the liquid. Coupling between translation and orientation is required since density fluctuations of an otherwise static random orientation distribution would not give rise to longitudinal polarization. Coupling of reorientation and translation has been observed in experiments studying flow and acoustic induced birefringence.[2,40,41] Another possibility is that there is a single, narrow, centered peak, and that a collective relaxation rather than a propagating mode is responsible for the VH spectrum. In either case, determination of the correlation length of the excitation will require measurement of the an-

gular variation of spectrally resolved HRS. The collective polar orientation correlations and fluctuations seen in HRS for water should also contribute to the dielectric response function.[42,43]

In conclusion, the polarization dependence of the HRS spectrum of water shows that molecular reorientation in water is predominantly a collective effect. The spectral widths show that the transverse and longitudinal reorientation modes fluctuate on time scales differing by at least a factor of 10.

## ACKNOWLEDGMENTS

The author thanks Matthew Eichenfield for help with sample preparation and polarization ratio measurements. This work was supported in part by the U.S. Army Research Office under Grant No. G-DAAD19-99-1-0086.

[1] B. J. Berne and R. Pecora, *Dynamic Light Scattering* (Wiley, New York, 1976).
[2] D. Kivelson and P. A. Madden, Annu. Rev. Phys. Chem. **31**, 523 (1980).
[3] G. D. Patterson and P. J. Carroll, J. Phys. Chem. **89**, 1344 (1985).
[4] V. N. Denisov, B. N. Mavrin, and V. B. Podobedov, Phys. Rep. **151**, 1 (1987).
[5] D. P. Shelton and P. Kaatz, Phys. Rev. Lett. **84**, 1224 (2000).
[6] D. P. Shelton, Chem. Phys. Lett. **325**, 513 (2000).
[7] D. P. Shelton, J. Opt. Soc. Am. B **17**, 2032 (2000).
[8] D. Eisenberg and W. Kauzmann, *The Structure and Properties of Water* (Oxford, New York, 1969).
[9] *Water: A Comprehensive Treatise*, edited by F. Franks (Plenum, New York, 1972), Vols. 1–7.
[10] P. Kaatz and D. P. Shelton, Rev. Sci. Instrum. **67**, 1438 (1996).
[11] P. Kaatz and D. P. Shelton, J. Chem. Phys. **105**, 3918 (1996).
[12] D. P. Shelton, Phys. Rev. A **42**, 2578 (1990).
[13] R. D. Pyatt and D. P. Shelton, J. Chem. Phys. **114**, 9938 (2001).
[14] V. Mazzacurati, A. Nucara, M. A. Ricci, G. Ruocco, and G. Signorelli, J. Chem. Phys. **93**, 7767 (1990).
[15] P. D. Maker, Phys. Rev. A **1**, 923 (1970).
[16] P. N. Butcher and D. Cotter, *The Elements of Nonlinear Optics* (Cambridge University Press, Cambridge, 1990).
[17] R. Bersohn, Y. H. Pao, and H. L. Frisch, J. Chem. Phys. **45**, 3184 (1966).
[18] J. Jerphagnon, D. Chemla, and R. Bonneville, Adv. Phys. **27**, 609 (1978).
[19] K. Altmann and G. Strey, J. Raman Spectrosc. **12**, 1 (1982).
[20] S. F. Hubbard, R. G. Petschek, K. D. Singer, N. D'Sidocky, C. Hudson, L. C. Chien, C. C. Henderson, and P. A. Cahill, J. Opt. Soc. Am. B **15**, 289 (1998).
[21] V. Ostroverkhov, R. G. Petschek, K. D. Singer, L. Sukhomlinova, R. J. Twieg, S.-X. Wang, and L. C. Chien, J. Opt. Soc. Am. B **17**, 1531 (2000).
[22] G. Maroulis, Chem. Phys. Lett. **289**, 403 (1998).
[23] Y. Luo, H. Agren, O. Vahtras, P. Jorgensen, V. Spirko, and H. Hettema, J. Chem. Phys. **98**, 7159 (1993).
[24] D. Spelsberg and W. Meyer, J. Chem. Phys. **108**, 1532 (1998).
[25] H. Sekino and R. J. Bartlett, J. Chem. Phys. **98**, 3022 (1993).
[26] D. M. Bishop, B. Kirtman, H. A. Kurtz, and J. E. Rice, J. Chem. Phys. **98**, 8024 (1993).
[27] P. Kaatz, E. A. Donley, and D. P. Shelton, J. Chem. Phys. **108**, 849 (1998).
[28] G. Maroulis, J. Chem. Phys. **113**, 1813 (2000).
[29] B. F. Levine and C. G. Bethea, J. Chem. Phys. **65**, 2429 (1976).
[30] K. V. Mikkelsen, Y. Luo, H. Agren, and P. Jorgensen, J. Chem. Phys. **102**, 9362 (1995).
[31] T. D. Poulsen, P. R. Ogilby, and K. V. Mikkelsen, J. Chem. Phys. **115**, 7843 (2001).
[32] A. V. Gubskaya and P. G. Kusalik, Mol. Phys. **99**, 1107 (2001).
[33] S. Kielich and M. Kozierowski, Acta Phys. Pol. A **45**, 231 (1974).
[34] G. E. Walrafen, J. Phys. Chem. **94**, 2237 (1990).
[35] G. E. Walrafen, M. S. Hokmabadi, W.-H. Yang, Y. C. Chu, and B. Monosmith, J. Phys. Chem. **93**, 2909 (1989).
[36] G. E. Walrafen, M. R. Fisher, M. S. Hokmabadi, and W.-H. Yang, J. Chem. Phys. **85**, 6970 (1986).
[37] F. Aliotta, C. Vasi, G. Maisano, D. Majolino, F. Mallamace, and P. Migliardo, J. Chem. Phys. **84**, 4731 (1986).
[38] G. Maisano, P. Migliardo, F. Aliotta, C. Vasi, F. Wanderlingh, and G. D'Arrigo, Phys. Rev. Lett. **52**, 1025 (1984).
[39] G. I. A. Stegeman and B. P. Stoicheff, Phys. Rev. A **7**, 1160 (1973).
[40] W. T. Grubbs and R. A. MacPhail, J. Chem. Phys. **97**, 8906 (1992).
[41] H. Nomura, S. Koda, and T. Matsuoka, *Memoirs of the School of Engineering* (Nagoya University, Nagoya, 1999), Vol. 51, p. 107.
[42] P. A. Bopp, A. A. Kornyshev, and G. Sutmann, J. Chem. Phys. **109**, 1939 (1998).
[43] B.-C. Perng and B. M. Ladanyi, J. Chem. Phys. **110**, 6389 (1999).